Engineering Geology 111 (2010) 19–30

Contents lists available at ScienceDirect

Engineering Geology

journal homepage: www.elsevier.com/locate/enggeo

A ground subsidence study based on DInSAR data: Calibration of soil parameters and subsidence prediction in Murcia City (Spain)

R. Tomás [a,*], G. Herrera [b], J. Delgado [a], J.M. Lopez-Sanchez [c], J.J. Mallorquí [d], J. Mulas [b]

[a] Departamento de Ingeniería de la Construcción, Obras Públicas e Infraestructura Urbana, Escuela Politécnica Superior, Universidad de Alicante P.O. Box 99, E-03080 Alicante, Spain
[b] Área de Investigación en Peligrosidad y Riesgos Geológicos, Departamento de Investigación y Prospectiva Geocientífica, Instituto Geológico y Minero de España (IGME), Ministerio de Ciencia y Tecnología, c/ Alenza 1, E-28003 Madrid, Spain
[c] Departamento de Física, Ingeniería de Sistemas y Teoría de la Señal (DFISTS), Escuela Politécnica Superior, Universidad de Alicante, P.O. Box 99, E-03080 Alicante, Spain
[d] Remote Sensing Lab., Departamento de Teoria del Senyal i Comunicacions, Universitat Politècnica de Catalunya, Campus Nord, Ed. D3, c/ Jordi Girona, 1-3, 08034 Barcelona, Spain

ARTICLE INFO

Article history:
Received 26 June 2009
Received in revised form 5 November 2009
Accepted 14 November 2009
Available online 2 December 2009

Keywords:
Subsidence
DInSAR
Model
Extensometer

ABSTRACT

Subsidence is a hazard that affects wide areas in the world causing important economic costs annually. The City of Murcia (SE Spain) is affected by this phenomenon since the 90s. In this work, ground subsidence caused by aquifer overexploitation is remotely monitored with Persistent Scatterer Interferometry (PSI). In particular, the so-called Coherent Pixels Technique (CPT) has been applied to SAR images from ERS and ENVISAT satellites. The CPT displacement time series corresponding to the 1993–1995 period have been used to calibrate a proposed one-dimensional subsidence model. Hence, the CPT time series have been successfully used to retrieve physical parameters of the soil. Then the model has been used to predict the deformations for the period 1993–2007. The comparison between the predictions of the model and the actual subsidence time series for the 1995–2007 period provides an average absolute difference of 3.2 ± 2.5 mm. Despite the simplicity of the adopted 1D model, these results show the usefulness of the CPT derived displacement information to calibrate and validate numerical models of ground subsidence due to aquifer overexploitation, which can be used to predict the aquifer's response for future piezometric falls.

1. Introduction

Ground subsidence induced by excessive exploitation of aquifers is a hazard affecting our society. This phenomenon is manifested at ground surface as millimetric to metric vertical displacements during periods that may last years, usually over wide areas. The problem of settlement is a critical issue for urban areas as it can lead to damages in human infrastructures causing important economic losses. It is estimated that there are over 150 cities in the world with serious problems of subsidence due to excessive groundwater withdrawal (Hu et al., 2004). Some well-known examples of subsidence around the world include the Po Valley (Italy), Mexico DC, Antelope, Santa Clara and San Joaquin Valleys (USA), Bangkok (Thailand) or Shanghai (China). In the metropolitan area of Murcia City (SE Spain) subsidence has occurred as a result of excessive pumping of groundwater, generating damages over 50 million euros and a significant social impact after the 1992–1995 drought period (Martínez et al., 2004).

Over the last decades Differential SAR Interferometry (DInSAR) has become an important remote sensing tool for detecting and monitoring ground surface displacements at a low cost with a millimetric precision. The simplest DInSAR technique was based on a single interferogram generated from a pair of SAR images (Rosen et al., 2000) and was applied to analyze subsidence due to ground water extraction in Galloway et al. (1998), Hoffmann et al. (2003) and Hoffman (2003). A remarkable improvement in the quality of the DInSAR results is given by a family of algorithms named Persistent Scatterer Interferometry (PSI) that are based on the simultaneous processing of multiple interferograms derived from a large set of SAR images (Ferretti et al., 2000; Berardino et al., 2002; Mora et al., 2003; Arnaud et al., 2003; Werner et al., 2003; Hooper et al., 2004). Subsidence monitoring applications of PSI can be found, for instance, in Ferretti et al. (2004), Tomás et al. (2005), Casu et al. (2006), Zerbini et al. (2007), Bell et al. (2008) and Herrera et al. (2009).

Diverse approaches have been proposed in the literature to predict land subsidence in order to care for societies affected by this phenomenon. These approaches can be classified following the Xu et al. (2008) criterion that divides subsidence prediction approaches into five categories: (a) Statistical method, as influence function, Gray theory and regression analysis; (b) one-dimensional numerical model; (c) quasi three-dimensional seepage model; (d) three-dimensional seepage, and (e) three-dimensional fully coupled models.

* Corresponding author.
E-mail addresses: roberto.tomas@ua.es (R. Tomás), g.herrera@igme.es (G. Herrera), jose.delgado@ua.es (J. Delgado), juanma.lopez@ua.es (J.M. Lopez-Sanchez), mallorqui@tsc.upc.edu (J.J. Mallorquí), j.mulas@igme.es (J. Mulas).

0013-7952/$ – see front matter © 2009 Elsevier B.V. All rights reserved.
doi:10.1016/j.enggeo.2009.11.004

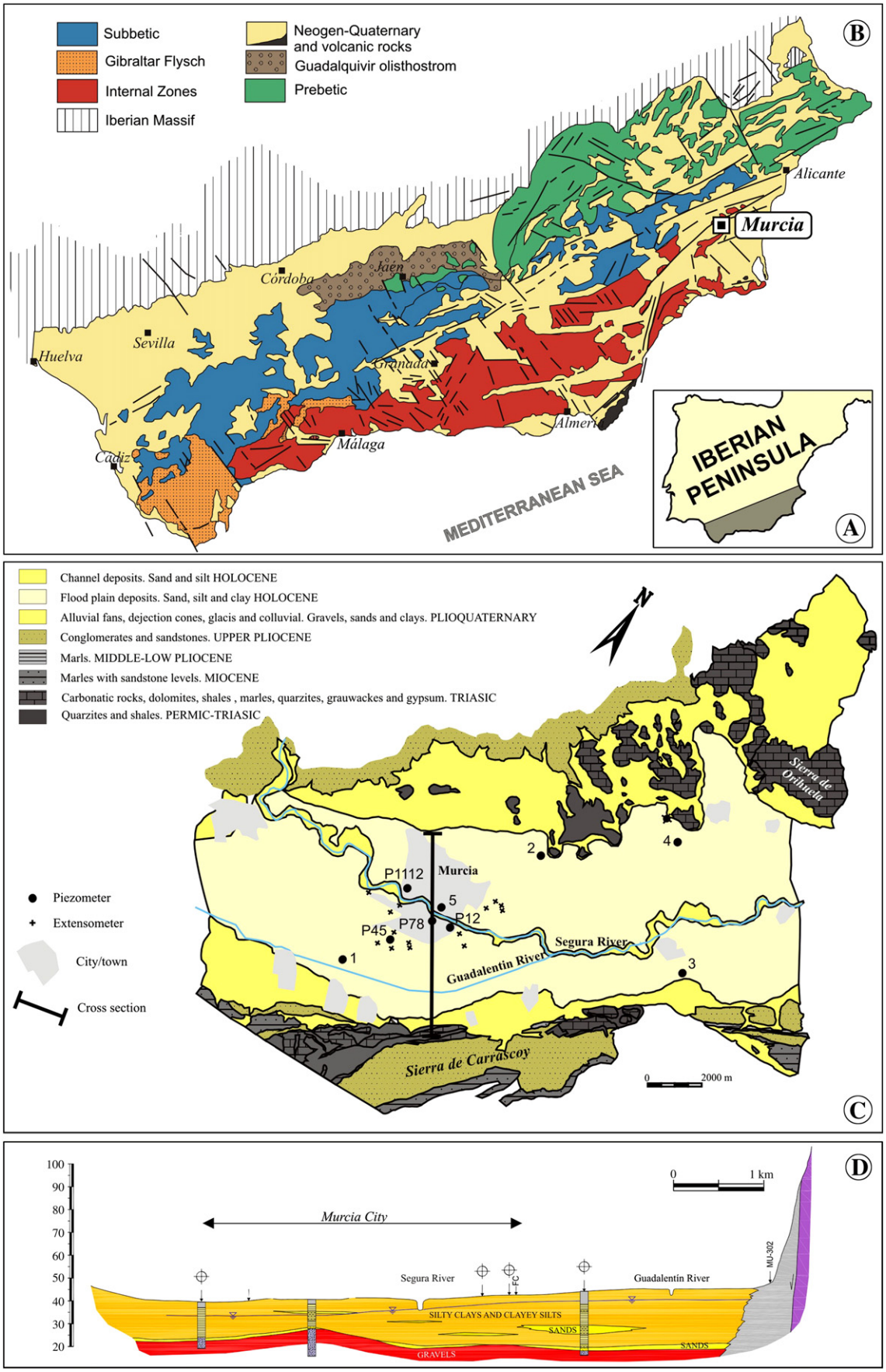

Fig. 1. Geological setting of the study area (based on Montenat (1977) and Aragón et al. (2004)). Piezometric levels for boreholes (1 to 5) and multipiezometers are shown in Figs. 2 and 3 respectively.

Fig. 2. Piezometric level temporal evolution at selected well points (see location in Fig. 1).

Statistical methods use simple relationships among subsidence and other factors (Gray theory model), water withdrawal volume or piezometric level (regression analysis method), or simply establish temporal trends of subsidence along time (influential functions). One-dimensional numerical method considers that piezometric level changes affecting aquifer and aquitard consolidation occur only in vertical direction. This method allows computing subsidence just at a point using only vertical soil parameters. Quasi three-dimensional seepage and three-dimensional seepage models use Terzaghi's one-dimensional consolidation equation (Terzaghi and Fröhlich, 1936) in order to compute subsidence. The difference between these two methods is due to the water flow seepage considered for aquifer and aquitard. The quasi three-dimensional seepage model considers that seepage in aquifer is horizontal and vertical for the aquitard, whereas the three-dimensional seepage model assumes that water flow develops in three dimensions. Finally, a three-dimensional fully coupled model simulates 3D water flow computing subsidence by means of Biot's 3D consolidation theory (Biot, 1941).

The selection of the most convenient model for predicting subsidence depends on several complex factors and on the local geological conditions, which can vary from place to place (Hu et al., 2002).

Subsidence prediction applications using these methods can be found for instance in Gambolati (1975), Helm (1975), Helm (1976), Gambolati et al. (1991), Monjoie et al. (1992), Mizumura (1994), Shearer (1998), Gambolati et al. (2001), Larson et al. (2001), Hu et al. (2002), Chen et al. (2003), Zhou et al. (2003), Don et al. (2005), Ferronato et al. (2007), Shi et al. (2007), Shi et al. (2008), Xue et al. (2008) and Wu et al. (2009).

In this paper, we focus our analysis on the subsidence occurring in Murcia City (SE Spain) by using the PSI method named Coherent Pixel Technique (CPT) (Mora et al., 2003; Blanco et al., 2008) and by employing images from the SAR sensors onboard of ERS and ENVISAT satellites. Previous works have already demonstrated and validated with in situ data the application of different PSI techniques, including CPT, in this area (Tomás et al., 2005; Herrera et al., 2008; Tomás, 2009). The present work is devoted to formulate a simple subsidence model and to apply it to this scenario as a prediction tool. The model will be both calibrated and validated using interferometry-derived data time series in different periods, thus showing its potential for predicting future conditions.

The paper is organized as follows. Section 2 describes the geographical and geological setting of the study area. Subsidence data obtained from interferometry are presented and briefly commented in Section 3. Then, Section 4 is devoted to present the proposed model for subsidence prediction, including its formulation, constants calibration, and validation with the available time series of data. The main conclusions are summarized in Section 5.

2. Geographical and geological setting

The Vega Media of the Segura River (VMSR) is located in the Eastern sector of the Betic Cordillera, in the so-called Bajo Segura basin (Montenat, 1977; Fig. 1). The nature of the materials outcropping along the boundaries of the valley varies depending on the site (Fig. 1C). The Southern border of the VMSR consists of rocks of the basin basement (Permian to Triassic in age). Meanwhile, the Northern border consists of sedimentary rocks (Upper Miocene to Pliocene) deposited in the basin (marls, sandstones and conglomerates). The materials found in the valley are recent (Holocene at ground surface, Pleistocene to Pliocene at some depth) sediments deposited by the Segura and Guadalentín rivers.

These recent sediments are very compressible and the most problematic from a geotechnical point of view. Rodríguez Jurado et al. (2000) and Mulas et al. (2003) made a geotechnical characterization of all these materials for the VMSR. Their models show that the same sedimentary rocks outcropping at the valley borders are also found at some depth within the valley and are characterized by low to negligible compressibility. Above them, the recent, surficial sediments are characterized by moderate to high compressibility.

The VMSR is also part of the so-called "Guadalentín–Segura Quaternary aquifer System No. 47" (IGME, 1986). This aquifer is characterized by two units (Cerón and Pulido, 1996; Aragón et al., 2004): a surface unit that consists on a semiconfined aquifer or aquitard formed by silty clays and clayey silts with sand intercalations (Fig. 1D), and a second one, or "deep aquifer", consisting on a multilayer aquifer composed of fine sand and gravels confined by silts and clay layers. The water table of the surface unit is found a few meters below ground surface. Due to the high fine content of

sediments, this aquifer is characterized by low hydraulic conductivity, so it is scarcely exploited. Consequently, water level shows small seasonal changes of a few meters maximum (Fig. 2).

In this case horizontal and vertical hydraulic conductivities of the second unit vary typically between 10–100 m/day and 1–50 m/day (Aragón et al., 2004). This second unit has several levels of gravels of hydrological interest. The most exploited is that which is located at the top of this unit, about 20 m below the surface (Fig. 1D). Its piezometric level is found a few meters below the ground surface and shows significant variations over time due to overexploitation in drought periods (Fig. 2). This was especially noticeable during the period 1992–1995, where peak values of piezometric level decline reached −15 m (Fig. 2). As a consequence, widespread subsidence affected the VMSR, causing damage to structures and a great public concern (Mulas et al., 2003; Martínez et al., 2004). Tomás et al. (2005, 2006), Tomás, (2009) and Herrera et al. (2008, 2009) measured such ground subsidence in the metropolitan area of Murcia during this drought period by means of differential SAR interferometry, detecting maximum displacements of 12 cm in the zone. Other layers of gravels of interest from a hydrological point of view are found at greater depths of this unit, but little is known about them.

Mulas et al. (2003) proposed a model to characterize and simulate the subsidence occurred due to the 1992–1995 drought. According to this model, subsidence occurs when water is pumped from the topmost layer of gravels of the deep aquifer. A vertical gradient is created that causes a downward flow of ground water from the upper aquifer (surface unit) towards the gravel layer causing a water table decline. Consequently, pore pressure in the superficial aquifer falls and the aquifer suffers a consolidation process.

The excess pore pressure dissipation rate is a key question for subsidence computation. Permeability laboratory tests taken under five undisturbed silty and clayey samples show very low and variable permeability values (from 8.20×10^{-11} to 6.24×10^{-8} m/s). As a consequence, a slow consolidation process is expected. In this sense, the multipiezometers installed in Murcia City by the Confederación Hidrográfica del Segura (CHS, 2007) in order to measure the aquitard and aquifer layer piezometric level (Fig. 3) show very similar response of both layers probably due to the existence of sand layers that favour water drainage (Fig. 3). Fig. 4 shows the lithological description of the hydrogeological boreholes drilled for multipiezometer installation. Although the lithological description of this type of boreholes is not very detailed, several sand layers intercalated (P78 in Fig. 4) or immediately over the gravels (P45 and P1112 in Fig. 4) have been

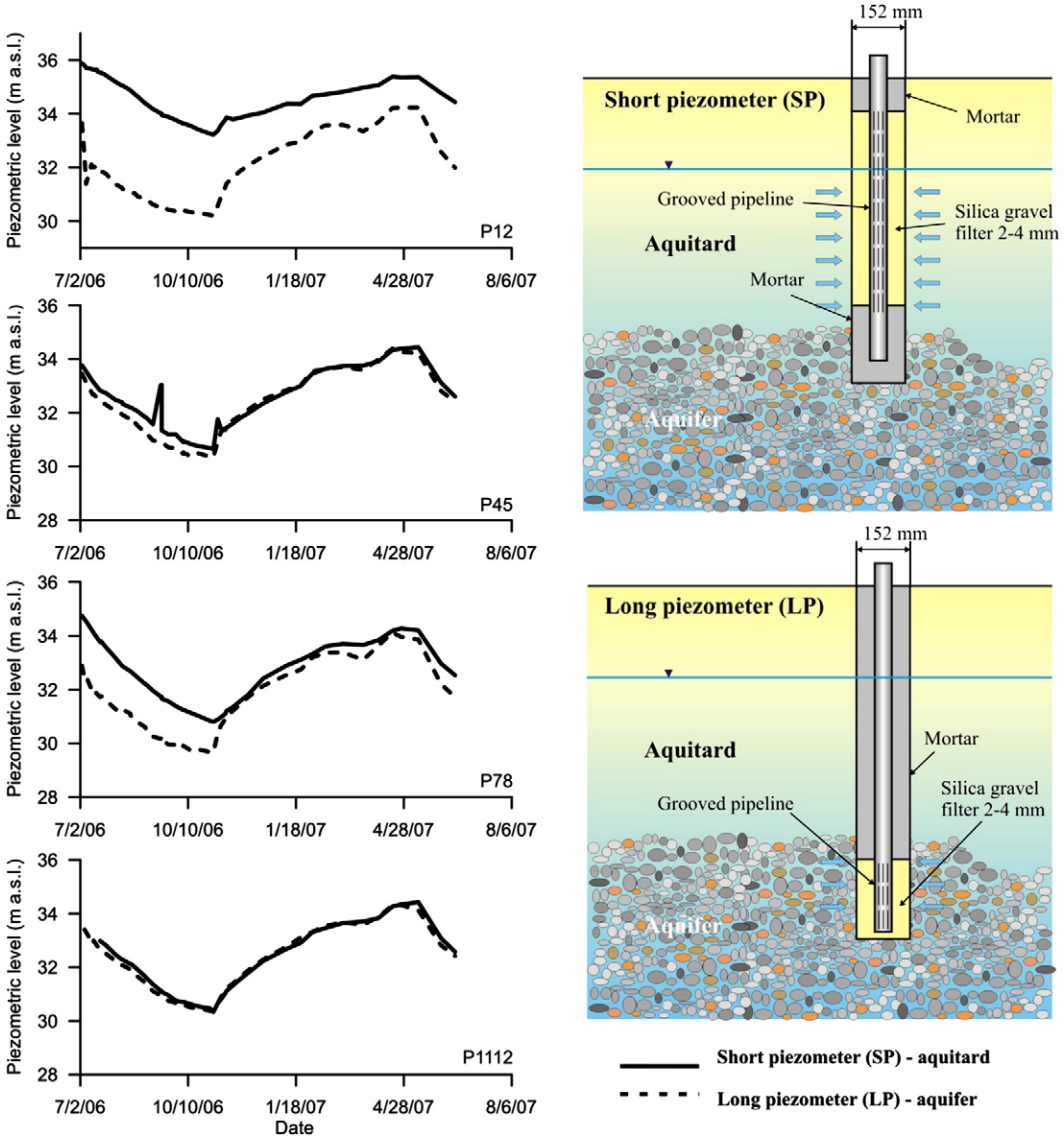

Fig. 3. Temporal evolution of piezometric level and installation scheme of multilevel piezometers of the city of Murcia. See lithological column and location of multilevel piezometer boreholes in Figs. 4 and 1 respectively.

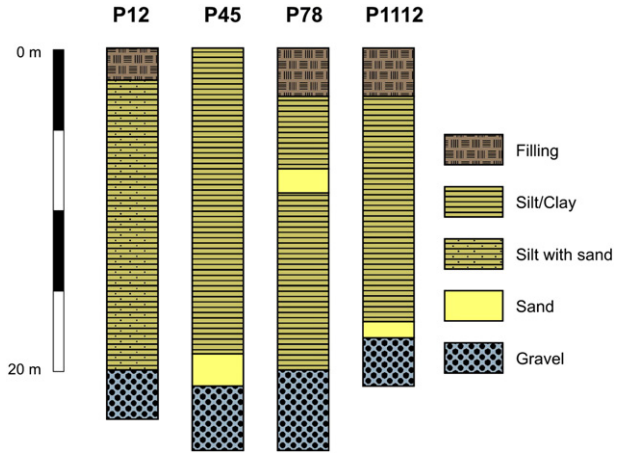

Fig. 4. Lithological columns of multilevel piezometers. See temporal evolution of piezometric level in Fig. 3.

recognized. Moreover, P12 and P1112 boreholes are composed by "silts with sands" that provide higher values of permeability to the clayey aquitard.

3. Subsidence data

In this work, ground subsidence measurements were obtained with a PSI technique called Coherent Pixels Technique (CPT). A detailed description of the technique can be found in Mora et al. (2003) and Blanco et al. (2008) but a summary is included here for the sake of completeness.

3.1. Methodology overview

The differential interferometric phase ($\Delta\psi_{int}$) obtained by combining two complex SAR images can be expressed as (Hanssen, 2001):

$$\Delta\psi_{int} = \Delta\psi_{flat} + \Delta\psi_{topo} + \Delta\psi_{mov} + \Delta\psi_{atmos} + \Delta\psi_{noise} \quad (1)$$

where $\Delta\psi_{flat}$ is the flat-earth component related to range distance differences in the absence of topography, $\Delta\psi_{topo}$ is the topographic phase, $\Delta\psi_{mov}$ is the phase contribution due to ground changes occurring between the two SAR image acquisitions, measured along the satellite Line of Sight (LOS), $\Delta\psi_{atmos}$ is the phase component due to atmospheric artifacts, and $\Delta\psi_{noise}$ includes the residual noise sources. The first two terms in Eq. (1) can be expressed analytically. In particular, $\Delta\psi_{flat}$ is easily known, and $\Delta\psi_{topo}$ can be computed from an external DEM.

The CPT algorithm (Mora et al., 2003) assumes that the phase component linked to deformation ($\Delta\psi_{mov}$) can be divided into two new phase terms, one due to linear deformation ($\Delta\psi_{linear}$), i.e. deformation at a constant rate over the whole period, and another due to non-linear deformation ($\Delta\psi_{non\text{-}linear}$). Consequently, the application of CPT is divided into two main steps corresponding to the extraction of both linear and non-linear deformation terms. The retrieval of the linear term includes the estimation of both the mean velocity of deformation and the DEM error. This estimation is carried out by adjusting a model function only over those pixels of the scene that show good interferometric coherence over time. Then, the non-linear term is extracted by applying a cascade of space–time filters to remove the contribution of atmospheric artifacts and to identify the low and high-resolution components of the non-linear deformation. Atmospheric isolation is possible, up to some extent, due to the different behavior of atmospheric artifacts in time and space when compared to the non-linear deformation contribution.

A couple of additional comments about the CPT processing are in order. First, the combined use of images from different sensors (ERS and ENVISAT) is possible through the computation of different subsets of interferograms generated among images of the same sensor (without crossed interferograms) and by linking the deformation results under a singular value decomposition approach, as explained in Blanco et al. (2005, 2008). Second, the absence of valid images during some periods (e.g. years 1994 and 2001) is solved both by increasing the maximum allowed temporal baseline of the interferograms (e.g. 3 years) in order to connect acquisitions before and after the data gaps, and by enlarging the time window used in the temporal filter in the presence of data gaps. In this way, despite the absence of measurement data at some time intervals, the whole time series is constructed consistently. This approach is valid under the assumption of a mostly linear deformation, as the one observed in Murcia.

3.2. Dataset and processing details

The SAR dataset analyzed in this work consists of a total of 81 images from ERS-1 (6 images), ERS-2 (56 images) and ENVISAT-ASAR (19 images), acquired from April 1993 to March 2007. A list of the images is shown in Table 1. A crop of about 10×10 km was extracted for processing, corresponding to the urban area of Murcia. Among all the total amount of possible interferograms formed by pairs of SAR images, only 185 interferograms have been selected for the CPT processing by means of a Delauney triangulation in the 3D space formed by the spatial baselines, temporal baselines and Doppler centroid differences. This selection has been restricted to those

Table 1
ERS and ENVISAT-SAR SLC data used for the analyzed period 1993–2007.

Nr.	Date	Sensor	Nr.	Date	Sensor
1	19930414	ers1	42	20011117	ers2
2	19930623	ers1	43	20020406	ers2
3	19931110	ers1	44	20020824	ers2
4	19950721	ers1	45	20021102	ers2
5	19950826	ers2	46	20021207	ers2
6	19950930	ers2	47	20030322	envi
7	19951104	ers2	48	20030809	ers2
8	19960706	ers2	49	20031018	envi
9	19961019	ers2	50	20031122	ers2
10	19970412	ers2	51	20040306	envi
11	19970517	ers2	52	20040515	envi
12	19970726	ers2	53	20040724	ers2
13	19970830	ers2	54	20040828	ers2
14	19971004	ers2	55	20041002	ers2
15	19971108	ers2	56	20041106	ers2
16	19980117	ers2	57	20041211	ers2
17	19980328	ers2	58	20050115	envi
18	19980711	ers2	59	20050219	envi
19	19980919	ers2	60	20050326	envi
20	19981128	ers2	61	20050430	envi
21	19990313	ers2	62	20050604	envi
22	19990522	ers2	63	20050604	ers2
23	19990730	ers1	64	20050709	ers2
24	19990731	ers2	65	20050813	envi
25	19990903	ers1	66	20050813	ers2
26	19990904	ers2	67	20050917	envi
27	19991009	ers2	68	20051126	envi
28	19991113	ers2	69	20051126	ers2
29	19991218	ers2	70	20051231	envi
30	20000122	ers2	71	20060311	ers2
31	20000226	ers2	72	20060415	envi
32	20000401	ers2	73	20060624	envi
33	20000506	ers2	74	20060624	ers2
34	20000610	ers2	75	20060729	ers2
35	20000715	ers2	76	20061007	envi
36	20000819	ers2	77	20061111	ers2
37	20001028	ers2	78	20070331	envi
38	20001202	ers2	79	20061111	ers2
39	20010106	ers2	80	20070331	envi
40	20010908	ers2	81	20070331	envi
41	20011013	ers2			

interferograms with spatial and temporal baselines smaller than 250 m and 1000 days, respectively, and Doppler centroid differences below 800 Hz. The external DEM used to cancel out the topographic component of the interferometric phase has a resolution of 25 m × 25 m and belongs to the cartographic numeric database E20 from IGN (National Cartographical Service of Spain). The selection of pixels where ground deformation information will be available has been performed using a multilayer coherence criterion consisting on selecting only those pixels where coherence is above a certain threshold for most of the interferograms (in this case 0.6, 0.5 and 0.4 respectively for at least 40% of the interferograms set). Among other advantages, this multilayer approach enables the computation of subsidence for low quality pixels because they take benefit of those with higher quality previously processed (Blanco et al., 2006, 2008). Coherence computation implies a spatial averaging of the interferograms, also known as multi-looking, that degrades the original resolution of the SAR images. In this work, a multi-look operation of 15 pixels in azimuth by 3 pixels in range has been used, thus providing a final resolution of 60 m × 60 m on ground.

3.3. DInSAR processing results and validation

Fig. 5 shows the total deformation (LOS displacement) map of the City of Murcia obtained for the period 1993–2007 superimposed on an aerial image. An average density of 76 coherent pixels per square kilometer has been obtained.

As it can be seen, subsidence is higher in the South and East of the city, with values greater than 5 cm for the whole period, whereas to the North a more stable situation is observed.

Before using the subsidence estimates for other purposes, they have been validated by comparing them against in situ extensometer measurements. From February 2001 to March 2007, fifteen extensometers (5 incremental and 10 rod extensometers) with a monitoring depth of about 15 m provided subsidence measurements. All rod extensometers were anchored at depths of 10 and 15 m. Incremental extensometers provide deformation measurements at intervals of 1 m. Both types of extensometers provide measurements with 0.1 mm accuracy.

The CPT accuracy has been assessed by comparing the retrieved deformations from the SAR data analysis with those available from the extensometer network measurements projected along the Line of Sight. In order to ease the comparison, LOS-projected extensometer time series have been interpolated within the interval common to the SAR images, i.e. from 2000 to 2007. The comparison with the extensometers has been done calculating two quality parameters: (1) the mean and standard deviation of the absolute difference between CPT and LOS-projected extensometer deformation time series (4.5 ± 4.1 mm), and (2) the mean and standard deviation of the

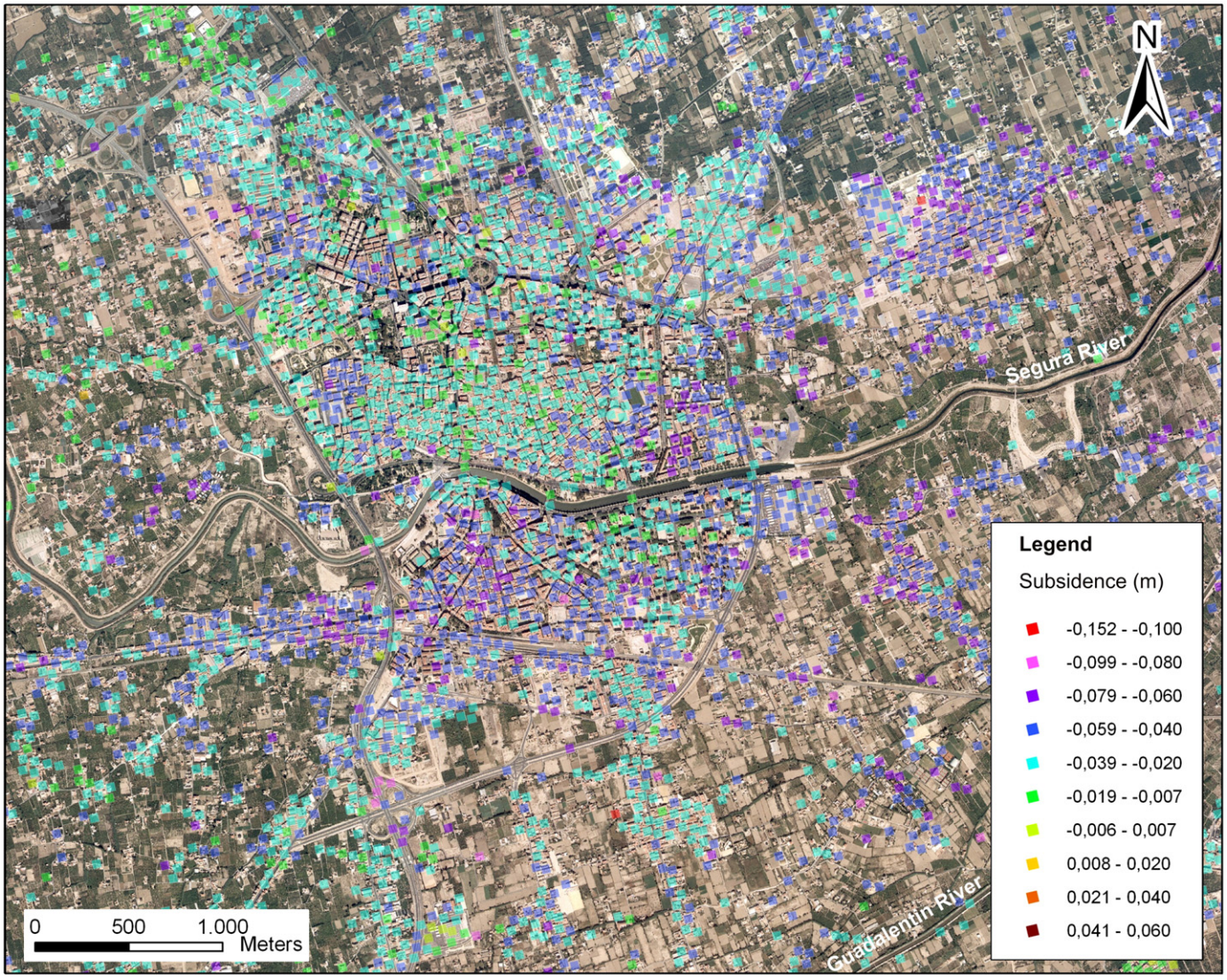

Fig. 5. LOS-projected subsidence map of the City of Murcia obtained by means of CPT technique corresponding to 1993–2007 period.

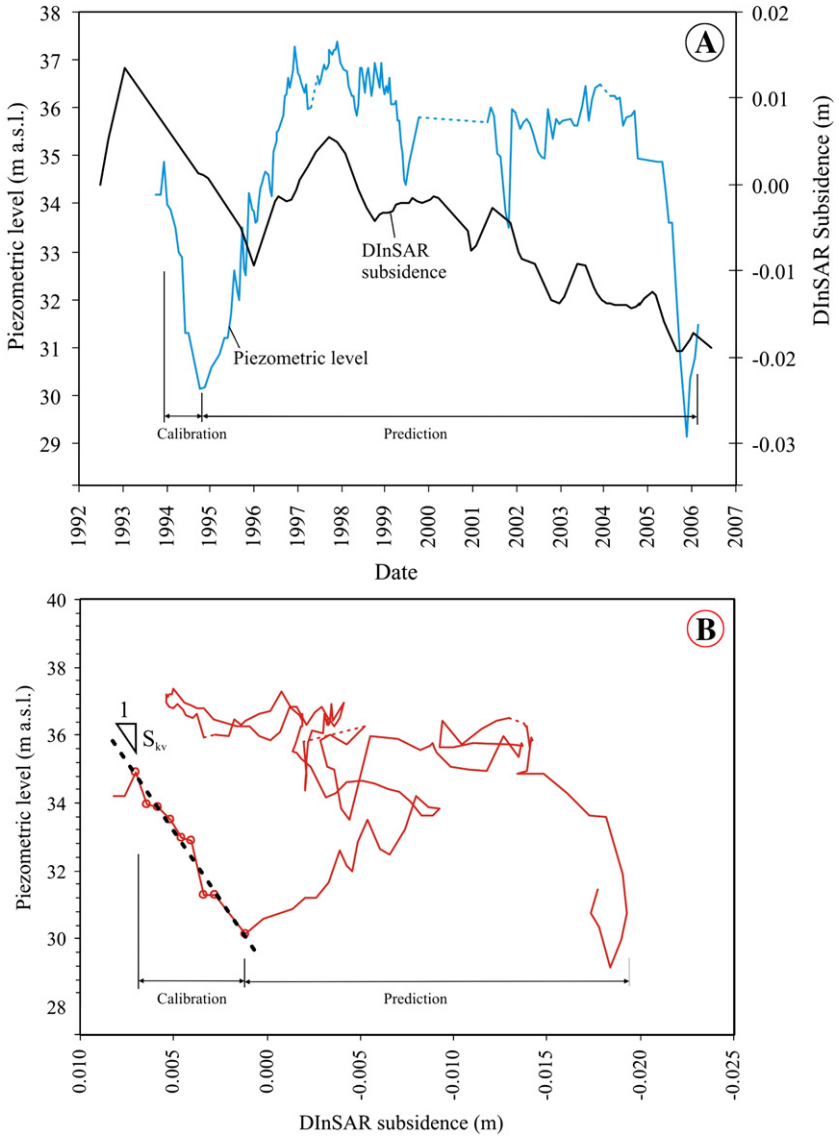

Fig. 6. A) LOS-projected subsidence and piezometric data used for the calibration and prediction. B) Strain–stress curve and graphical construction for anelastic coefficient computation.

difference between CPT and LOS-projected extensometer deformation time series (-2.6 ± 4.7 mm). These values are in agreement with the ones obtained by other authors in similar experiments (see Strozzi et al. (2001), Hanssen (2003), Colesanti et al. (2003), Casu et al. (2006), Crosetto et al. (2008), and Herrera et al. (2009)).

4. Subsidence computation

In this paper, a one-dimensional model has been used for modeling subsidence due to piezometric level changes. This model assumes that deformations are directly caused by vertical effective stress changes derived from piezometric level changes and that aquitard pore pressure equilibrates instantaneously with the piezometric level changes of the gravels layer. Notice that the assumption of an instantaneous propagation of the pressure decline within the aquifer–aquitard column implies that no consolidation occurs when the piezometric level is stable. As it was verified in Section 2, this assumption can be accepted for this case of study.

Murcia City covers several square kilometers, being the considered depth of the study area about 15 m. Available data are insufficient to build a full three-dimensional flow and subsidence analysis. This is the principal reason why several one-dimensional analyses have been chosen instead of a global model of the aquifer–aquitard system.

Next subsections show: a) the model calibration process for aquitard deformation parameters computation using DInSAR data corresponding to 1993–95 period; b) the implementation of the model for subsidence history prediction at several wells and; c) the validation of the subsidence predictions comparing model subsidence estimates and 1995–2007 DInSAR data.

4.1. Model calibration

The evaluation of ground settlement is a common task in geotechnical engineering. In this case, settlement is evaluated by considering three kinds of parameters: (i) thickness of potentially deformable soil, (ii) variation of stress state, and (iii) a modulus relating the two previous parameters. We consider that changes in stress state are due to variations in water table position. Consequently, this relationship can be written as:

$$\delta = \Delta h \times S_{sk} \times D = \Delta h \times S_k \tag{2}$$

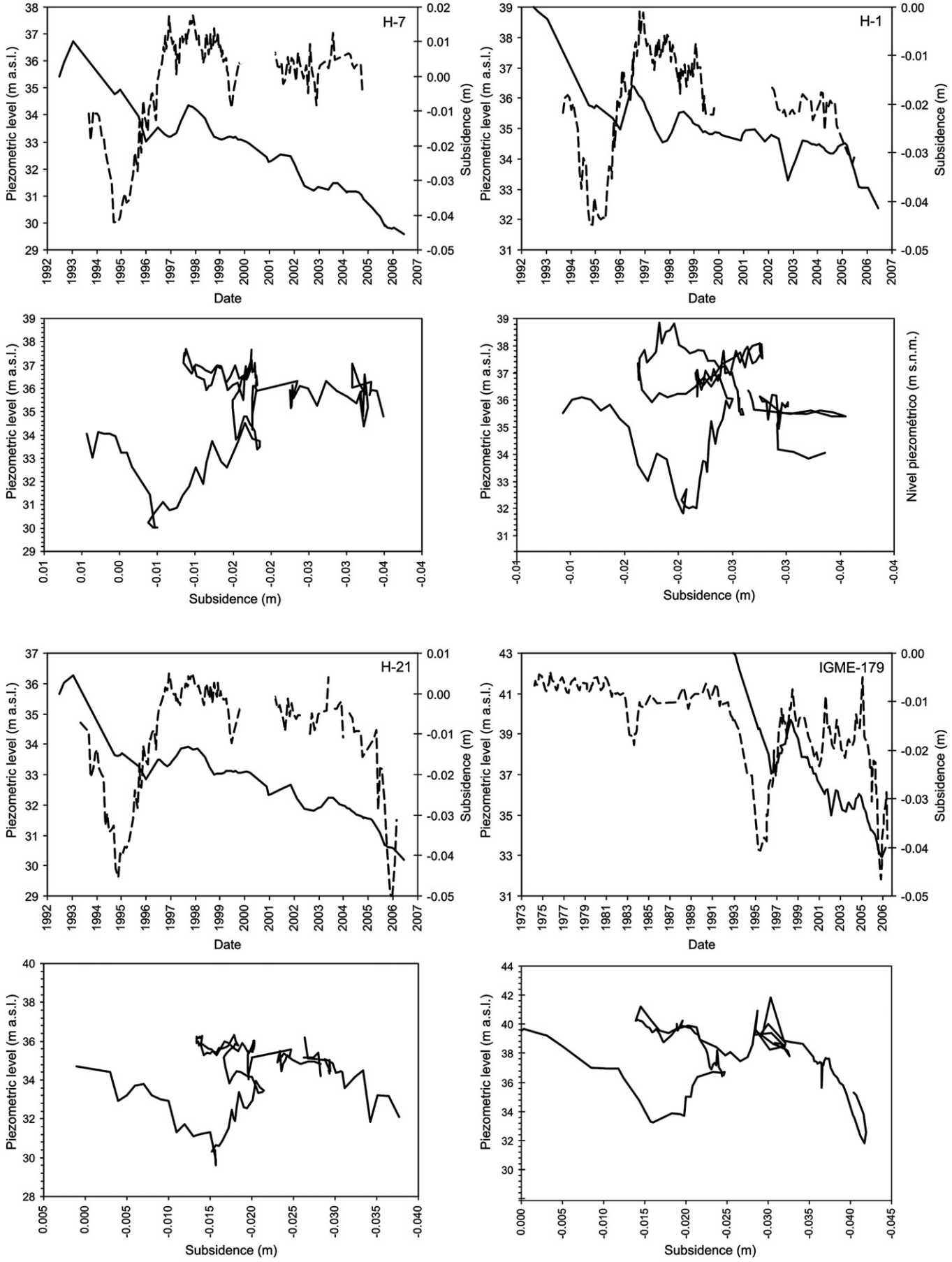

Fig. 7. Piezometric level evolution versus LOS-projected DInSAR subsidence and stress–strain curves for several wells.

where δ is the subsidence (m), D is the deformable soil thickness (m), Δh is the piezometric level decrease (m), S_{sk} is the specific storage coefficient of the aquitard (m^{-1}), and S_k is the storage coefficient (dimensionless) of the aquitard. S_k or S_{sk} represents the deformability of the aquitard and varies with the stress state. It adopts a different value depending on the piezometric level (H) and its position above or below the maximum recorded piezometric decline (H_p). Therefore, H_p is equivalent to the well-known soil preconsolidation stress used in geotechnical engineering that represents the maximum effective stress suffered by soil. This value separates the elastic recoverable deformations from the unelastic, unrecoverable, deformations:

$$S_k = \begin{cases} S_{ke} \text{ if } H > H_p \\ S_{kv} \text{ if } H < H_p \end{cases}. \quad (3)$$

Notice that the definition of specific elastic storage implies that water is incompressible. This statement is valid for unconsolidated alluvial aquifer systems where typically storage coefficient is higher than storage coefficient owing to the compressibility of the pore pressure (Galloway and Hoffmann, 2007).

Aquitard anelastic storage coefficients S_{kv} have been computed using piezometric series for 24 available wells where DInSAR retrieved deformations are also known (Figs. 6 and 7). These data allow us to draw stress–strain curves that represent the relationship between piezometric level changes and aquitard deformations (Figs. 6 and 7). The graphical methodology proposed by Riley (1969) has been used to compute anelastic storage coefficients (Fig. 6B and Table 2) and, therefore, to calibrate the model. This methodology has been used by several authors (Hoffman, 2003; Hoffmann et al., 2003; Bubey, 2003; Tomás et al., 2006; Galloway and Hoffmann, 2007; Zhang et al., 2007a,b) and consists in determining the slope of the branch of the stress–strain curve (elastic or anelastic):

$$S_k = \frac{\Delta D}{\Delta h} \quad (4)$$

where ΔD is the subsidence caused by a Δh piezometric level decrease.

The 1993–95 piezometric fall is the first maximum known decrease occurred in the VMSR. As a consequence, the storage coefficient calculated for this period is considered to be anelastic. This assumption is justified because this piezometric level drop reduces significantly pore pressure, thus producing the maximum effective stress increase in the aquitard history.

The computed anelastic storage coefficients (S_{kv}) for the available wells of the City of Murcia vary from 4.900×10^{-4} to 3.058×10^{-3}, with an average value of $1.513\times10^{-3}\pm0.680\times10^{-3}$ (Table 2).

The elastic storage coefficient (S_{ke}) has been computed as a percentage of anelastic storage coefficient (S_{kv}). For this purpose the ratio between the swelling index (C_s) – slope of the oedometric unloading–reloading branch – and the compression index (C_c) – slope of the oedometric virgin compression branch –, C_s/C_c, that are comparable to S_{ke} and S_{kv} parameters, has been obtained from 139 oedometric tests performed following the UNE 103-405-94 (UNE, 1994) procedure. The estimated C_s/C_c ratio is 15%. Computed values for anelastic and elastic storage coefficients for the Murcia City are shown in Table 2 and vary from 7.350×10^{-5} to 4.587×10^{-4}, with an average value of $2.269\times10^{-4}\pm1.020\times10^{-4}$.

4.2. Model implementation

Once the S_{kv} and the S_{ke} have been computed for each well, the next step consists in the extrapolation of the data to the rest of the piezometric level time series in order to verify the consistency of the model. Therefore, this extrapolation is equivalent to a prediction of future scenarios, but with the key advantage of data being available to validate predictions. Due to the hydrogeological simplicity of subsiding aquitard, for this task a one-dimensional method has been applied.

First, the preconsolidation piezometric level (H_p) has to be established in order to distinguish elastic from anelastic deformations due to piezometric level changes. This piezometric level has been determined as the minimum piezometric level corresponding to seasonal fluctuations. Table 2 shows the H_p values determined for every available well. The model assumes that the whole deformable soil column at every well has the same H_p value. This assumption is in

Table 2
Anelastic (S_{kv}) and elastic (S_{ke}) storage coefficients, preconsolidation piezometric level (H_p) and errors of the model for 1995–2007 period. CP: Coherent pixel.

Well	CP-well distance (m)	S_{kv}	S_{ke}	H_p (m a.s.l.)	$\varepsilon\pm\sigma$ (mm)	$\lvert\varepsilon\rvert\pm\lvert\sigma\rvert$ (mm)	Maximum series error (mm)
H-1	75.64	1.743×10^{-3}	2.615×10^{-4}	37	0.1 ± 2.6	2.0 ± 1.7	6.3
H-2	10.16	1.319×10^{-3}	1.978×10^{-4}	36	0.7 ± 3.0	2.1 ± 2.3	8.7
H-4	65.19	1.002×10^{-3}	1.503×10^{-4}	37	3.0 ± 3.4	3.9 ± 2.3	8.3
H-6	40.56	1.903×10^{-3}	2.855×10^{-4}	35	-3.2 ± 4.3	4.3 ± 3.3	14.4
H-7	31.82	1.835×10^{-3}	2.753×10^{-4}	36	3.1 ± 4.3	4.3 ± 3.1	11.3
H-8	17.51	9.570×10^{-4}	1.435×10^{-4}	37	5.6 ± 3.3	5.6 ± 3.3	11.4
H-11	45.91	1.538×10^{-3}	2.308×10^{-4}	36	0.1 ± 4.2	3.5 ± 2.3	10.0
H-16	20.59	1.539×10^{-3}	2.308×10^{-4}	37	-0.6 ± 2.3	1.8 ± 1.5	5.7
H-19	46.19	1.113×10^{-3}	1.669×10^{-4}	36	1.8 ± 3.5	3.3 ± 2.3	10.4
H-20	30.63	1.462×10^{-3}	2.194×10^{-4}	37	-0.4 ± 2.5	2.1 ± 1.5	5.7
H-21	41.31	2.982×10^{-3}	4.473×10^{-4}	35	-1.7 ± 2.9	2.4 ± 2.3	13.0
H-25	36.49	1.358×10^{-3}	2.037×10^{-4}	37	0.6 ± 3.2	2.5 ± 2.0	7.9
H-26	62.79	1.077×10^{-3}	1.616×10^{-4}	37	2.5 ± 6.2	5.7 ± 3.6	13.7
H-27	46.13	1.201×10^{-3}	1.802×10^{-4}	39	2.7 ± 2.9	3.0 ± 2.6	8.4
H-33	47.68	4.900×10^{-4}	7.35×10^{-5}	40	2.6 ± 4.9	3.8 ± 4.0	15.4
H-34	24.68	1.968×10^{-3}	2.952×10^{-4}	37	1.4 ± 2.1	2.0 ± 1.6	7.5
H-38	70.83	1.457×10^{-3}	2.186×10^{-4}	35	-0.9 ± 3.8	3.6 ± 1.7	6.3
H-39	102.87	2.380×10^{-3}	3.571×10^{-4}	36	-1.1 ± 4.1	3.6 ± 2.3	8.2
H-42	29.12	7.69×10^{-4}	1.154×10^{-4}	35	-1.7 ± 5.5	5.1 ± 2.6	11.9
H-44	20.24	1.013×10^{-3}	1.520×10^{-4}	35	0.2 ± 1.8	1.4 ± 1.2	4.7
H-45	43.97	1.035×10^{-3}	1.553×10^{-4}	36	2.3 ± 2.8	2.8 ± 2.3	9.3
H-46	39.08	6.410×10^{-4}	9.620×10^{-5}	39	3.5 ± 3.3	3.8 ± 2.9	8.3
H-55	29.07	3.058×10^{-3}	4.587×10^{-4}	36	-0.5 ± 3.7	3.1 ± 2.2	8.6
IGME179	47.64	2.461×10^{-3}	3.691×10^{-4}	39	0.1 ± 6.9	5.6 ± 4.0	16.9
Average	42.75	1.513×10^{-3}	2.269×10^{-4}	37	0.8 ± 3.6	3.4 ± 2.5	9.7
Minimum	10.16	4.900×10^{-4}	7.350×10^{-5}	–	-3.2	1.4	4.7
Maximum	102.87	3.058×10^{-3}	4.587×10^{-4}	–	5.6	5.7	16.9

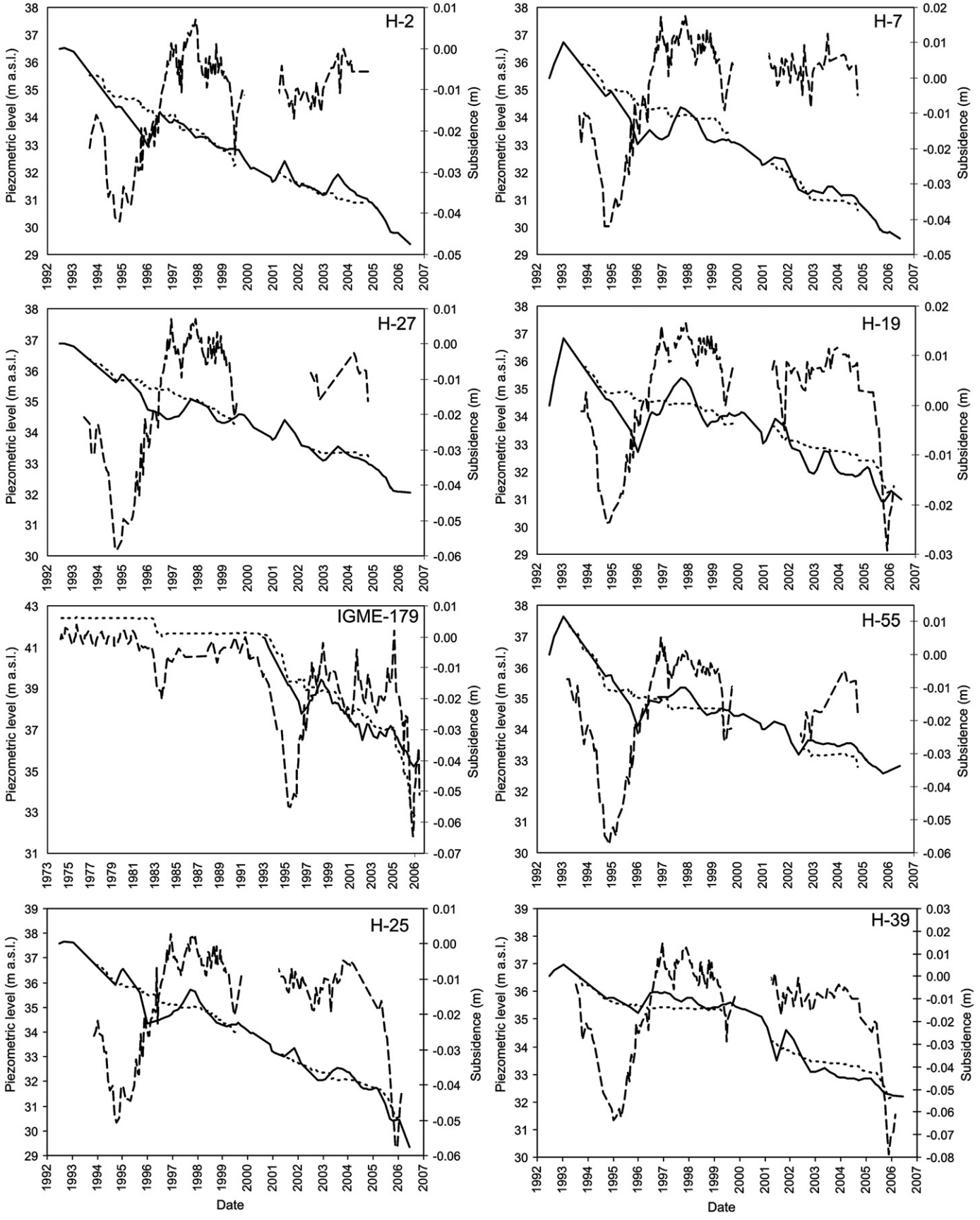

Fig. 8. Model prediction results. Dashed line: piezometric level. Continuous line: DInSAR deformation. Dotted line: modeled subsidence.

agreement with the preconsolidation values calculated by Tomás et al. (2007) that demonstrate that close to the ground surface, the soil is highly overconsolidated above the water table and normally consolidated below this level.

Taking into account the parameters calculated for each well in the previous section, subsidence has been estimated using expression (2). Subsidence evolution ($\delta(t)$) has been computed between 1993 and 2007 as the sum of the partial deformations (δ_i) calculated for each piezometric change (Δh_i).

Notice that Eq. (2) assumes the instantaneous equilibration of the heads in the aquitard with the head in the lower aquifer. This assumption is a reasonable simplification for thin aquitards (Leighton and Phillinps, 2003; Galloway and Hoffmann, 2007). Fig. 8 shows the results of the subsidence prediction obtained using the proposed formulation.

4.3. Model validation

The model previously defined has been used to simulate subsidence in the period 1993–2007 where SAR images are available. Fig. 8 shows the modeling results at the location of several wells. These results have been employed for testing the self-consistency of the model.

The average difference between DInSAR and modeling time series and its deviation has been defined as a quality indicator of the fit between both series. The absolute error corresponds to the average absolute difference between the same time series data. Table 2 shows the comparison between the modeling and actual DInSAR data.

Taking into account the 24 wells analyzed in this work, the average error of the model for the period 1995–2007 is 0.8 ± 3.6 mm, with extreme values of -3.2 and 5.6 mm (Table 2). This error is computed as the average of the differences between predicted subsidence values and DInSAR subsidence values for each date of the analyzed temporal series. The average absolute error, computed using the absolute differences between the model deformations and the DInSAR subsidence data, is 3.4 ± 2.5 mm with extreme (maximum and minimum) values of 5.7 and 1.4 mm respectively for all the wells population. These results are similar to those obtained by Herrera et al. (2009) that computed average values of the absolute difference between their numerical model and DInSAR time series of displacement of 5.5 ± 4.7 mm.

5. Conclusions

In this work, the joint use of subsidence time series obtained by differential SAR interferometry and piezometric data for 1993–1997 period has provided aquifer system soil deformation parameters in the Murcia City. Obtained parameters are anelastic (S_{kv}) and elastic (S_{ke}) storage coefficients. These soil parameters have been used for a simply subsidence forecast. The used subsidence prediction model considers soil thickness and piezometric level changes as conditioning and triggering subsidence factors, respectively and has permitted to simulate subsidence evolution between 1993 and 2007. Obtained results projected along LOS have been validated by comparison with DInSAR 1995–2007 period measurements of the displacement. The average values of the absolute differences between model and DInSAR time series of deformation for 24 wells in the City of Murcia are 3.2 ± 2.5 mm. These results demonstrate that PSI DInSAR techniques are a useful tool to study scenarios with subsidence induced by piezometric level changes related to aquifer overexploitation providing soil deformation modulus that can be used for subsidence prediction.

Acknowledgements

The SAR images used in this work were provided by the European Space Agency (ESA) in the framework of the EO Cat. 1-2494 project. This study was partially funded by the Spanish Ministry of Science and Technology and EU FEDER (Project TEC-2008-06764) and by the University of Alicante (Projects VIGROB-157 and VIGROB-184). The Instituto Geológico y Minero de España (IGME) and EMUASA were kind enough to provide piezometric and hydrological data. Finally, the authors want to thank anonymous reviewers for the important contributions to this work.

References

Aragón, R., García-Aróstegui, J.L., Lambán, J., Hornero, J., Fernández-Grillo, A.I. (2004). Impacto de la explotación intensiva de aguas subterráneas en la ciudad de Murcia (España). Análisis hidrogeológico. Proc. XXXIII Congress of IAH-ALHSUD, Conf. on Groundwater Flow Understand. from local to regional scales, Zacatecas, Mexico, 11–15 October (on CD ROM).

Arnaud, A., Adam, N., Hanssen, R., Inglada, J., Duro, J., Closa, J., Eineder, M., 2003. ASAR ERS interferometric phase continuity. Proc. IEEE International Geoscience and Remote Sensing Symposium (IGARSS-03), 21–25 July, Toulouse, France, vol. 2, pp. 1133–1135.

Bell, J.W., Amelung, F., Ferretti, A., Bianchi, M., Novali, F., 2008. Permanent scatterer InSAR reveals seasonal and long-term aquifer-system response to groundwater pumping and artificial recharge. Water Resour. Res. 44, 1–18.

Berardino, P., Fornaro, G., Lanari, R., Sansosti, E., 2002. A new algorithm for surface deformation monitoring based on small baseline differential SAR interferograms. IEEE Trans. Geosci. Remote Sens. 40, 2375–2383.

Biot, M.A., 1941. General theory of three-dimensional consolidation. J. Appl. Phys. 12, 155–164.

Blanco, P., Mallorquí, J.J., Navarrete, D., Duque, S., Prats, P., Romero, R., Domínguez, J., Carrasco, D., 2005. Application of the Coherent Pixels Technique to the generation of deformation maps with ERS and ENVISAT data. Proc. IEEE International Geoscience and Remote Sensing Symposium (IGARSS-05), July, Seoul, Korea.

Blanco, P., Mallorquí, J.J., Duque, S., Navarrete, D., 2006. Advances on DInSAR with ERS and ENVISAT data using the Coherent Pixels Technique. Proc. IEEE International Geoscience and Remote Sensing Symposium (IGARSS-06), July, Denver, U.S.A.

Blanco, P., Mallorquí, J.J., Duque, S., Monells, D., 2008. The Coherent Pixels Technique (CPT): an advanced DInSAR technique for non-linear deformation monitoring. Pure Appl. Geophys. 165, 1167–1193.

Bubey, T.J., 2003. Use of time-subsidence data during pumping to characterize specific storage and hydraulic conductivity of semiconfining units. J. Hydrol. 281, 3–22.

Casu, F., Manzo, M., Lanari, R.A., 2006. Quantitative assessment of the SBAS algorithm performance for surface deformation retrieval from DInSAR data. J. Remote Sens. Environ. 102, 195–210.

Cerón, J.C., Pulido, A., 1996. Groundwater problems resulting from CO_2 pollution and overexploitation in Alto Guadalentín aquifer (Murcia, Spain). Environ. Geol. 28, 223–228.

Chen, C., Pei, S., Jiao, J.J., 2003. Land subsidence caused by groundwater exploitation in Suzhou City, China. Hydrogeol. J. 11, 275–287.

CHS (2007). Nuevas aportaciones al conocimiento hidrogeológico del entorno urbano de Murcia. 363 pp. Technical report. Available in: www.chs.es.

Colesanti, C., Ferretti, A., Prati, C., Rocca, F., 2003. Monitoring landslides and tectonic motions with the Permanent Scatterers Technique. Eng. Geol. 68, 3–14.

Crosetto, M., Biescas, E., Duro, J., Closa, J., Arnaud, A., 2008. Generation of advanced ERS and ENVISAT interferometric SAR products using stable point network technique. ASPRS J. Photogramm. Eng. Remote Sens. 74, 443–450.

Don, N.C., Araki, H., Yamanishi, H., Koga, K., 2005. Simulation of ground water flow and environmental effects resulting from pumping. Environ. Geol. 47, 361–374.

Ferretti, A., Prati, C., Rocca, F., 2000. Nonlinear subsidence rate estimation using permanent scatterers in differential SAR interferometry. IEEE Trans. Geosci. Remote Sens. 38, 2202–2212.

Ferretti, A., Novali, F., Bürgmann, R., Hilley, G., Prati, C., 2004. InSAR permanent scatterer analysis reveals ups and downs in San Francisco Bay Area. EOS 85, 317–324.

Ferronato, M., Mazzia, A., Pini, G., Gambolati, G., 2007. A meshless method for axisymmetric poroelastic simulations: numerical study. Int. J. Numer. Methods Eng. 70, 1346–1365.

Galloway, D.L., Hoffmann, J., 2007. The application of satellite differential SAR interferometry-derived ground displacements in hydrogeology. Hydrogeol. J. 15, 133–154.

Galloway, D.L., Hudnut, K.W., Ingebritsen, S.E., Philips, S.P., Peltzer, G., Rogez, F., Rosen, P.A., 1998. Detection of aquifer system compaction and land subsidence using interferometric synthetic aperture radar, Antelope Valley, Mojave Desert, California. Water Resour. Res. 34, 2573–2585.

Gambolati, G., 1975. Numerical models in land subsidence control. Comput. Methods Appl. Mech. Eng. 5, 227–237.

Gambolati, G., Ricceri, G., Bertoni, W., Bringhenti, G., Vuillermin, E., 1991. Mathematical simulation of the subsidence of Ravenna. Water Resour. Res. 27, 2899–2918.

Gambolati, G., Ferronato, M., Teatini, P., Deidda, R., Lecca, G., 2001. Finite element analysis of land subsidence above depleted reservoirs with pore pressure gradient and total stress formulations. Int. J. Numer. Anal. Methods Geomech. 25, 307–327.

Hanssen, R.F., 2001. Radar interferometry. Data Interpretation and Error Analysis. The Netherlands' Kluwer Academic Publisher. 308 pp.

Hanssen, R.F., 2003. Subsidence monitoring using contiguous and PSInSAR: quality assessment based on the precision and reliability. Proc. 11th FIG Sym. Def. Measur., Santorini, Greece.

Helm, D.C., 1975. One-dimensional simulation of aquifer system compaction near Pixley, California, part 1, constant parameters. Water Resour. Res. 11, 465–478.
Helm, D.C., 1976. One-dimensional simulation of aquifer system compaction near Pixley, California, part 2, stress-dependent parameters. Water Resour. Res. 12, 375–391.
Herrera, G., Fernandez-Merodo, J., Tomás, R., Cooksley, G., Mulas, J., 2009. Advanced interpretation of subsidence in Murcia (SE Spain) using A-DInSAR data-modelling and validation. Nat. Hazards Earth Syst. Sci. 9, 647–661.
Herrera, G., Tomás, R., Lopez-Sanchez, J.M., Delgado, J., Vicente, F., Mulas, J., Cooksley, G., Sanchez, M., Duro, J., Arnaud, A., Blanco, P., Duque, S., Mallorquí, J.J., De la Vega-Panizo, R., Monserrat, O., 2008. Validation and comparison of advanced differential interferometry techniques: Murcia Metropolitan Area case study. ISPRS J. Photogramm. Remote Sens 64, 501–512.
Hoffman, J. (2003). The application of satellite radar interferometry to the study of land subsidence over developed aquifer systems. PhD Thesis, University of Stanford, 211 pp.
Hoffmann, J., Galloway, D.L., Zebker, H.A., 2003. Inverse modeling of interbed storage parameters using land subsidence observations, Antelope Valley, California. Water Resour. Res. 39, 5–10.
Hooper, A., Zebker, H., Segall, P., Kampes, B., 2004. A new method for measuring deformation on volcanoes and other natural terrains using InSAR Persistent Scatterers. Geophys. Res. Lett. 31. doi:10.1029/2004GL021737.21.
Hu, R.L., Wang, S.J., Lee, C.F., Li, M.L., 2002. Characteristics and trends of land subsidence in Tanggu, Tianjin, China. Bull. Eng. Geol. Environ. 61, 213–225.
Hu, R.L., Yue, Z.Q., Wang, L.C., Wang, S.J., 2004. Review on current status and challenging issues of land subsidence in China. Eng. Geol. 76, 65–77.
IGME, 1986. Calidad de Las Aguas Subterráneas en la Cuenca Baja del Segura y Costeras de Alicante. Instituto Geológico y Minero Ed., Madrid.
Larson, K.J., Başağaoğlu, H., Mariño, M.A., 2001. Prediction of optimal safe ground water yield and land subsidence in the Banos-Kettleman City area, California, using a calibrated numerical simulation model. J. Hydrol. 242, 79–102.
Leighton, D.A., Phillinps, S.P., 2003. Simulation of ground-water flow and land subsidence in the Antelope Valley ground-water basin. California, U.S. Geol. Surv. Water Resour. Ivest. Rep. 03-4106.
Martínez, M., Mulas, J., Herrera, G., Aragón, R., 2004. Efectos de una subsidencia moderada por extracción de agua subterránea en Murcia, España. Proc. XXXIII Congress of IAH-ALHSUD, Conf. on Groundwater Flow Understanding from local to regional scales, Zacatecas, Mexico, 11–15 October (on CD ROM).
Mizumura, K., 1994. Prediction of land subsidence due to ground-water use in snow country. J. Hydraul. Eng. 120, 448–460.
Monjoie, A., Paepe, R., SU, H.U., 1992. Land subsidence in Shanghai (P.R. of China). Bull. Eng. Geol. Environ. 46, 5–7.
Montenat, C. (1977). Les basins néogènes et quaternaries du Levant d'Alicante à Murcie (Cordillères bétiques orientales, Espagne). Stratigrafphie, paléontologie et évolution dynamique. Docum. Lab. Géol., Univ. Lyon, 69, 345 pp.
Mora, O., Mallorquí, J.J., Broquetas, A., 2003. Linear and nonlinear terrain deformation maps from a reduced set of interferometric SAR images. IEEE Trans. Geosci. Remote 41, 2243–2253.
Mulas, J., Aragón, R., Martínez, M., Lambán, J., García-Arostegui, J.L., Fernández-Grillo, A.I., Hornero, J., Rodríguez, J., Rodríguez, J.M., 2003. Geotechnical and hydrological analysis of land subsidence in Murcia (Spain). Proc. of the 1st International Conf. on Ground water in Geotechnical Engineering, RMZ-M&G, Bled, Slovenia, 22–26 September, pp. 249–252.
Riley, F.S., 1969. Análisis of borehole extensometer data from central California. In: Tison, L.J. (Ed.), Land subsidence, vol. 2, pp. 423–431.
Rodríguez Jurado, J., Martínez Corbella, M., Mulas, J., Rodríguez Ortiz, J.M., 2000. Establecimiento de un modelo geológico para el estudio de la subsidencia por rebajamiento del nivel freático. Geotemas 1, 155–158.
Rosen, P.A., Hensley, S., Joughin, I.R., Li, F.K., Madsen, S.N., Rodríguez, E., Goldstein, R.M., 2000. Synthetic aperture radar interferometry. Proc. IEEE 88, 333–382.
Shearer, T.R., 1998. A numerical model to calculate land subsidence, applied at Hangu in China. Eng. Geol. 49, 85–93.
Shi, X., Xue, Y., Ye, S., Wu, J., Zhang, Y., Yu, J., 2007. Characterization of land subsidence induced by groundwater withdrawals in Su-Xi-Chang area, China. Environ. Geol. 52, 27–40.
Shi, X., Wu, J., Ye, S., Zhang, Y., Xue, Y., Wei, Z., Li, Q., Yu, J., 2008. Regional land subsidence simulation in Su-Xi-Chang area and Shanghai City, China. Eng. Geol. 100, 27–42.
Strozzi, T., Wegm¨uller, U., Tosi, L., Bitelli, G., Spreckels, V., 2001. Land subsidence monitoring with differential SAR interferometry. Photogramm. Eng. Remote Sensing 67, 1261–1270.
Terzaghi, K., Fröhlich, O.K., 1936. Theorie der Setzung von Tonschich ten. Deuticke, Vienna.
Tomás, R. (2009). Estudio de la subsidencia de la ciudad de Murcia mediante Interferometría SAR diferencial (DInSAR) avanzada. PhD Thesis.
Tomás, R., Márquez, Y., Lopez-Sanchez, J.M., Delgado, J., Blanco, P., Mallorqui, J.J., Martinez, M., Herrera, G., Mulas, J., 2005. Mapping ground subsidence induced by aquifer overexploitation using advanced Differential SAR Interferometry: Vega Media of the Segura River (SE Spain) case study. Remote Sensing of the Environment 98, 269–283.
Tomás, R., Lopez-Sanchez, J.M., Delgado, J., Mallorquí, J.J., 2006. Hydrological parameters of the Vega Media of the Segura River Aquifer (SE Spain) obtained by means of advanced DInSAR. IEEE International Conference on Geoscience and Remote Sensing Symposium, 2006 (IGARSS 2006), July 31–Aug. 4, pp. 1553–1556.
Tomás, R., Doménech, C., Mira, A., Cuencai, A., Delgado, J., 2007. Preconsolidation stress in the Vega Baja and Media areas of the River Segura (SE Spain): Causes and relationship with piezometric level changes. Eng. Geol. 91, 135–151.
UNE, 1994. Geotecnia, UNE 103-405-94. Ensayo de consolidación unidimensional de un suelo en edómetro, Asociación Española de Normalización y Certificación (AENOR), Madrid. 10pp.
Werner, C., Wegmüller, U., Strozzi, T., Wiesmann, A., 2003. Interferometric point target analysis for deformation mapping. Proc. IEEE International Geoscience and Remote Sensing Symposium (IGARSS-03), 21–25 July, Toulouse. France 7, 4362–4364.
Wu, J., Shi, X., Ye, S., Xue, Y., Zhang, Y., Yu, J., 2009. Numerical simulation of land subsidence induced by groundwater overexploitation in Su-Xi-Chang area. China. Environ. Geol. 57, 1409–1421.
Xu, Y., Shen, S., Cai, Z., Zhou, G., 2008. The state of land subsidence and prediction approaches due to ground water withdrawal in China. Nat. Hazards 45, 123–135.
Xue, Y., Wu, J., Zhang, Y., Ye, S., Shi, X., Wei, Z., Li, Q., Yu, J., 2008. Simulation of regional land subsidence in the southern Yangtze Delta. Sci. China, Ser. D Earth Sci. 51, 808–825.
Zerbini, S., Richter, B., Rocca, F., Van Dam, T., Matonti, F., 2007. A combination of space and terrestrial geodetic techniques to monitor land subsidence: case study, the Southeastern Po Plain, Italy. J. Geophys. Res. 112, B05401. doi:10.1029/2006JB004338.
Zhang, Y., Xue, Y.-Q., Wu, J.-C., Ye, S.-J., Wei, Z.-W., Li, Q.-F., Yu, J., 2007a. Characteristics of aquifer system deformation in the Southern Yangtse Delta. China. Eng. Geol. 90, 160–173.
Zhang, Y., Xue, Y.-Q., Wu, J.-C., Ye, S.-J., Li, Q.-F., 2007b. Stress–strain measurements of deforming aquifer system that underlie Shanghai, China. Environ. Eng. Geosci. XIII, 217–228.
Zhou, G., Esaki, T., Mori, J., 2003. GIS-based spatial and temporal prediction system development for regional land subsidence hazard mitigation. Environ. Geol. 44, 665–678.